

Fig. 1. Conductance of half wave dipole as a function of wire radius  $a$ . The reference data are from [12].

TABLE III  
HALF WAVE DIPOLE ADMITTANCE

wire radius $a/\lambda$	$Y(mS)$	diff <sup>(1)</sup>
0.1	$11.6012 + 6.8476j$	0.12
0.025	$8.4327 - 0.4191j$	0.07
$6.25 \times 10^{-3}$	$8.1783 - 3.4363j$	0.03
$1.56 \times 10^{-3}$	$8.6140 - 4.6439j$	0.05
$3.91 \times 10^{-4}$	$9.0410 - 5.1264j$	0.12
<sup>(1)</sup> relative difference with [12] ( $\times 10^{-2}$ )		

## V. CONCLUSION

Fast and accurate algorithms for the potential of a uniform charge distribution on a flat cylinder have been presented. They were implemented in a low order, and therefore computationally efficient, full kernel thin wire code, based on the EFIE, to model the charge accumulation on the wire end caps. A range of linear dipoles with varying wire radius and a fixed length of  $\lambda/2$  was analysed and the results showed good correspondence with those of a recent high order MFIE model from the literature. It is further noteworthy that, in spite of the linear discretization, even a 40 segment model showed quite accurate results (0.2% difference with the reference). The latter model has 39 bilinear cylindrical basis functions plus two end caps, amounting to 41 unknowns in total.

## ACKNOWLEDGMENT

The authors would like to thank the authors of [12] for giving them the necessary data for Fig. 1 and Table III.

## REFERENCES

- [1] R. F. Harrington, *Field Computation by Moment Methods*. New York: MacMillan, 1968.
- [2] B. D. Popovic, M. B. Dragovic, and A. R. Djordjevic, *Analysis and Synthesis of Wire Antennas*. Chichester, U.K.: U.K. Research Studies Press, 1982.
- [3] C. Puente, J. Romeu, R. Pous, J. Ramis, and A. Hijazo, "Small but long Koch fractal monopole," *IEE Electron. Lett.*, vol. 34, no. 1, pp. 9–10, Jan. 1998.
- [4] E. Ozbay, K. Aydin, E. Cubukcu, and M. Bayindir, "Transmission and reflection properties of composite double negative metamaterials in free space," *IEEE Trans. Antennas Propag.*, vol. 51, no. 10, pp. 2592–2595, Oct. 2003.

- [5] S. Park and C. Balanis, "Efficient kernel calculation of cylindrical antennas," *IEEE Trans. Antennas Propag.*, vol. 43, no. 11, Nov. 1995.
- [6] D. H. Werner, "A method of moments approach for the efficient and accurate modeling of moderately thick cylindrical wire antennas," *IEEE Trans. Antennas Propag.*, vol. 46, no. 3, pp. 373–382, Mar. 1998.
- [7] A. Heldring and J. M. Rius, "Efficient full-kernel evaluation for thin wire analysis," *Microw. Opt. Technol. Lett.*, vol. 44, no. 5, pp. 477–480, March 2005.
- [8] B. M. Kolundzija, "Effect of a wire end in thin-wire analysis," in *AP-S Digest*, 1988, vol. 2, pp. 843–846.
- [9] C. D. Taylor and D. R. Wilton, "The extended boundary condition solution of the dipole antenna of revolution," *IEEE Trans. Antennas Propag.*, vol. 20, no. 6, pp. 772–776, Nov. 1972.
- [10] E. H. Newman, "A unified theory of thin material wires," *IEEE Trans. Antennas Propag.*, vol. 39, no. 10, Oct. 1991.
- [11] A. G. Tijhuis, P. Zhongqiu, and A. Rubio Bretones, "Transient excitation of a straight thin wire segment: a new look at an old problem," *IEEE Trans. Antennas Propag.*, vol. 40, no. 10, Oct. 1992.
- [12] A. F. Peterson and M. M. Bibby, "High order numerical solutions of the MFIE for the linear dipole," *IEEE Trans. Antennas Propag.*, vol. 52, no. 10, pp. 2684–2991, Oct. 2004.
- [13] M. Abramowitz and I. A. Stegun, Eds., *Handbook of Mathematical Functions* 9th printing. New York, Dover, 1972.
- [14] H. Lass and L. Blitzer, "The gravitational potential due to uniform disks and rings," *Celestial Mechanics*, vol. 30, pp. 225–228, 1983.
- [15] C. Hastings, *Approximations for Digital Computers*. Princeton, NJ: Princeton Univ. Press, 1955.
- [16] B. C. Carlson, "Numerical computation of real or complex elliptic integrals," *Numerical Algorithms*, vol. 10, pp. 13–26, 1995.
- [17] J. Binney and S. Tremaine, *Galactic Dynamics*. Princeton, NJ: Princeton Univ. Press, 1987.

## Polar Integration for Exact Space-Time Quadrature in Time-Domain Integral Equations

James Pingenot, Swagato Chakraborty, and Vikram Jandhyala

**Abstract**—A space-time polar quadrature technique for numerical integration of Green's function interactions in time-domain integral equations is presented. The method transforms 2-D surface space-time integrals associated with vector and scalar potentials to a 1-D integral that is performed using Gauss-Legendre integration. The advantage of the presented technique compared to standard 2-D Gaussian quadrature is that time delays between each section of the source basis function and the observation point are accounted for exactly in an analytic manner. This ensures highly accurate temporal behavior of the Green's function interactions thereby contributing to the stability of the overall time-domain integral equations.

**Index Terms**—BEM, integral equations, integration, quadrature, time domain.

## I. INTRODUCTION

Time-domain integral equations (TDIEs) are now powerful and rapidly evolving tools for temporal simulation of electromagnetic behavior of complex structures. Several researchers have recently developed techniques for enhancing stability. In addition to techniques for stability such as special basis functions [1]–[3] and implicit schemes [4], it is also imperative to have accurate space-time quadrature schemes. Compared to frequency-domain quadrature, TDIE integration has the additional property of requiring exact time delays

Manuscript received August 22, 2005; revised April 16, 2006.

The authors are with the Electrical Engineering Department, University of Washington, Seattle, WA 98105 USA (e-mail: pingej@u.washington.edu).

Digital Object Identifier 10.1109/TAP.2006.882195

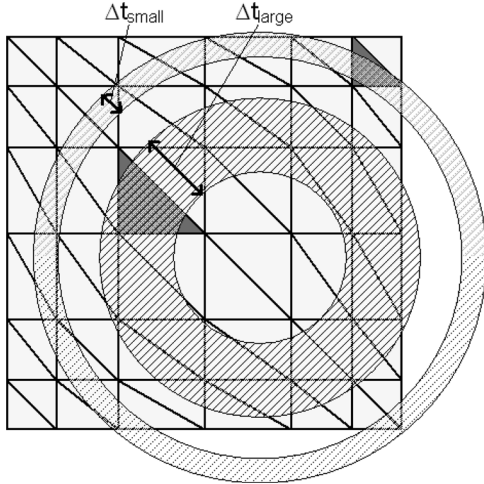


Fig. 1. Mesh of plate, with swept element size. If the time step is chosen as implicit for the large element, important interactions will be missed in the the lumping together of small elements. On the other hand, if the integration is not performed exactly, the small time step will be unstable for the larger elements.

between each point in a source region and the observer location. The standard approximation to this is multipoint 2-D quadrature [5] with analytical singularity extraction [6], while the Duffy method [7], Nyström method [8], the method presented recently by Khayat and Wilton [9], and methods for conformal elements [10] have been used for more exact integration. However, no study to date has examined how the shape of potential interactions affects the stability of the system. It has been assumed that accurate integration of the spatial component (while accounting for delays) will provide accurate temporal resolution. We find this is not so.

This is of particular importance when meshes have been refined, and both electrically-large and electrically-small elements are present on the same mesh, as shown in Fig. 1. In this case, a large time step misses important interactions taking place between small elements. However, if the time step is small, the equations for large elements become explicit, leading to instability in the solution. The resolution to this problem is to use a small time step, but to accurately integrate the space-time quadrature of a TDIE system to retain stability for the larger elements.

In this paper, the exact space integrals for vector and scalar potentials for frequency-domain developed in [11] are adapted to the space-time integrals of the time-domain. This method is chosen because it is optimized to accurately predict the temporal shape of potential interactions. The 2-D integration of free-space Green's functions are converted to piecewise smooth 1-D integrals over delay (with a 1-D analytical integration) via a polar transformation, that can easily be addressed by Gauss-Legendre integration. This simple and elegant transformation allows arbitrary accuracy in delay calculations. As shown by the examples, this technique greatly enhances potential accuracy, which may lead to more stable and accurate TDIE codes. The quadrature technique can be applied directly to all integrations: singular, near-singular, close-range, and far-field integrals, arising in different sections of the TDIE matrices. The goal of this paper is to show that the delay integration is key to accurate potential calculation. As will be seen in the results, inaccurate potential integration creates spurious high-frequency signals capable of destabilizing TDIE codes. At present this method is limited to planar elements, but may be adapted to conformal elements in the future.

Section II of this paper describes the formulation of polar integration in the time-domain. Section III compares polar integration to Gaussian

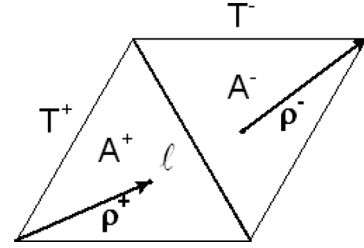


Fig. 2. RWG basis function over two triangles,  $T^+$  and  $T^-$ .

quadrature for predicting vector and scalar potentials due to a Rao-Wilton-Glisson (RWG) type function [12] on a single triangle.

## II. FORMULATION

The magnetic vector potential,  $\mathbf{A}(\mathbf{r})$ , and electric scalar potential,  $\phi(\mathbf{r})$ , due to a current density,  $\mathbf{J}(\mathbf{r}, t)$ , and charge density,  $q(\mathbf{r}, t)$ , on a surface  $S$ , are given by

$$\mathbf{A}(\mathbf{r}) = \frac{\mu}{4\pi} \int_S \frac{\mathbf{J}\left(\mathbf{r}', t - \frac{|\mathbf{r}-\mathbf{r}'|}{c}\right)}{|\mathbf{r}-\mathbf{r}'|} ds \quad (1)$$

$$\phi(\mathbf{r}) = \frac{1}{4\pi\epsilon} \int_S \frac{q\left(\mathbf{r}', t - \frac{|\mathbf{r}-\mathbf{r}'|}{c}\right)}{|\mathbf{r}-\mathbf{r}'|} ds \quad (2)$$

where the quantities  $\epsilon$ ,  $\mu$ , and  $c$  are the background material's permittivity, permeability, and propagation velocity, respectively. The current and charge are related by the continuity equation

$$\nabla \cdot \mathbf{J}(\mathbf{r}, t) + \dot{q}(\mathbf{r}, t) = 0. \quad (3)$$

Following the method used in [1], the current and charge can be written in terms of the same unknown

$$\mathbf{J}(\mathbf{r}, t) = \dot{\mathbf{P}}(\mathbf{r}, t) \quad (4)$$

$$q(\mathbf{r}, t) = -\nabla \cdot \mathbf{P}(\mathbf{r}, t). \quad (5)$$

Substituting (4) and (5) into (1) and (2) gives

$$\mathbf{A}(\mathbf{r}) = \frac{\mu}{4\pi} \int_S \frac{\dot{\mathbf{P}}\left(\mathbf{r}', t - \frac{|\mathbf{r}-\mathbf{r}'|}{c}\right)}{|\mathbf{r}-\mathbf{r}'|} ds \quad (6)$$

$$\phi(\mathbf{r}) = -\frac{1}{4\pi\epsilon} \int_S \frac{\nabla \cdot \mathbf{P}\left(\mathbf{r}', t - \frac{|\mathbf{r}-\mathbf{r}'|}{c}\right)}{|\mathbf{r}-\mathbf{r}'|} ds. \quad (7)$$

The surface is tessellated, and the spatial behavior of the current is characterized by RWG basis functions over adjacent, paired triangles,  $T^+$  and  $T^-$

$$\mathbf{P}(\mathbf{r}, t) = \begin{cases} \frac{l}{2A^\pm} \boldsymbol{\rho}^\pm P(t), & \mathbf{r} \in T^\pm \\ 0, & \mathbf{r} \notin T^\pm \end{cases} \quad (8)$$

where  $l$  is the length of the shared edge between the triangles and  $A^\pm$  is the area of the source triangle. The vector  $\boldsymbol{\rho}^\pm$  is the vector from (to) the node opposite the shared edge to (from)  $\mathbf{r}$  on  $T^+$  ( $T^-$ ). Fig. 2 depicts this basis function. The quantity  $P(t)$  characterizes the temporal behavior of  $\mathbf{P}(\mathbf{r}, t)$ . The integration of a basis function over a single triangle can now be described as

$$\mathbf{A}(\mathbf{r}) = \frac{\mu}{4\pi} \frac{l}{2A^\pm} \int_T \frac{\boldsymbol{\rho}^\pm \dot{P}\left(t - \frac{|\mathbf{r}-\mathbf{r}'|}{c}\right)}{|\mathbf{r}-\mathbf{r}'|} ds \quad (9)$$

$$\phi(\mathbf{r}) = -\frac{1}{4\pi\epsilon} \frac{l}{A^\pm} \int_T \frac{P\left(t - \frac{|\mathbf{r}-\mathbf{r}'|}{c}\right)}{|\mathbf{r}-\mathbf{r}'|} ds. \quad (10)$$

The key to polar quadrature is taking the surface integration in 3-D space, and transforming it into a 2-D integration in the plane of the source function. The transformation is characterized by

$$\boldsymbol{\rho}^{\pm} = \boldsymbol{\rho} - \boldsymbol{\rho}^c \quad (11)$$

$$R = \sqrt{\rho^2 + d^2} \quad (12)$$

$$ds = \rho d\rho d\theta \quad (13)$$

where  $d$  is the distance from the observation point to its projection on the plane of the triangle,  $\boldsymbol{\rho}$  is the vector from the projection point to the source point,  $\boldsymbol{\rho}^c$  is the vector from the projection point to the origin-node of the RWG basis function, and  $\rho = |\boldsymbol{\rho}|$ . Note that  $\boldsymbol{\rho}^c$  is constant with respect to the integration.

The potentials can then be written as

$$\mathbf{A}(\mathbf{r}) = \frac{\mu}{4\pi} \frac{l}{2A^{\pm}} \left[ \dot{\mathbf{M}}_{vect} - \boldsymbol{\rho}^c \dot{M}_{scal} \right] \quad (14)$$

$$\phi(\mathbf{r}) = -\frac{1}{4\pi\epsilon} \frac{l}{A^{\pm}} M_{scal} \quad (15)$$

where

$$\mathbf{M}_{vect} = \iint \frac{\rho^2 (\hat{\mathbf{u}} \cos \theta + \hat{\mathbf{v}} \sin \theta) P \left( t - \frac{\sqrt{\rho^2 + d^2}}{c} \right)}{\sqrt{\rho^2 + d^2}} d\rho d\theta \quad (16a)$$

$$M_{scal} = \iint \frac{\rho P \left( t - \frac{\sqrt{\rho^2 + d^2}}{c} \right)}{\sqrt{\rho^2 + d^2}} d\rho d\theta. \quad (16b)$$

In (16a) the local vector  $\boldsymbol{\rho}$  has been broken down into its local Cartesian components as  $\boldsymbol{\rho} = \hat{\mathbf{u}} \cos \theta + \hat{\mathbf{v}} \sin \theta$ . The temporal derivatives of  $P(t)$  in (14) are left for analytical evaluation.

The above integrals can be described by

$$I_{\varphi\chi} = \int_{\rho} \int_{\theta} \varphi(\rho) \chi(\theta) d\rho d\theta. \quad (17)$$

The function  $\varphi$  is defined as either  $\varphi_{M,vect}$  or  $\varphi_{M,scal}$  where

$$\varphi_{M,vect}(\rho) = \frac{\rho^2 P \left( t - \frac{\sqrt{\rho^2 + d^2}}{c} \right)}{\sqrt{\rho^2 + d^2}} \quad (18a)$$

$$\varphi_{M,scal}(\rho) = \frac{\rho P \left( t - \frac{\sqrt{\rho^2 + d^2}}{c} \right)}{\sqrt{\rho^2 + d^2}}. \quad (18b)$$

If  $d = 0$  (as in the singular case), these become

$$\varphi_{M,vect}(\rho) = \rho P \left( t - \frac{\rho}{c} \right) \quad (19a)$$

$$\varphi_{M,scal}(\rho) = P \left( t - \frac{\rho}{c} \right) \quad (19b)$$

which is non-singular. The function  $\chi$  is either  $\chi_c = \cos(\theta)$ ,  $\chi_s = \sin(\theta)$  or  $\chi_0 = 1$ .

Now that the integrand has been separated into functions of the two variables, the integrals may be dealt with separately. The limits of the integration in  $\theta$  depend on the value of  $\rho$ . As illustrated in Fig. 3, the circle defined by  $\rho$  can intersect a triangle between zero and six places, creating between one and three intervals to analytically integrate in  $\theta$ . If there are zero intersection points, the interval is  $(0, 2\pi)$ . We define

$$\begin{pmatrix} \xi_c(\rho) \\ \xi_s(\rho) \\ \xi_0(\rho) \end{pmatrix} = \sum_{i=1}^{K(\rho)} \int_{\theta_{min}^i(\rho)}^{\theta_{max}^i(\rho)} \begin{pmatrix} \cos \theta \\ \sin \theta \\ 1 \end{pmatrix} d\theta \\ = \sum_{i=1}^{K(\rho)} \begin{bmatrix} \sin \theta_{max}^i(\rho) - \sin \theta_{min}^i(\rho) \\ -\cos \theta_{max}^i(\rho) + \cos \theta_{min}^i(\rho) \\ \theta_{max}^i(\rho) - \theta_{min}^i(\rho) \end{bmatrix} \quad (20)$$

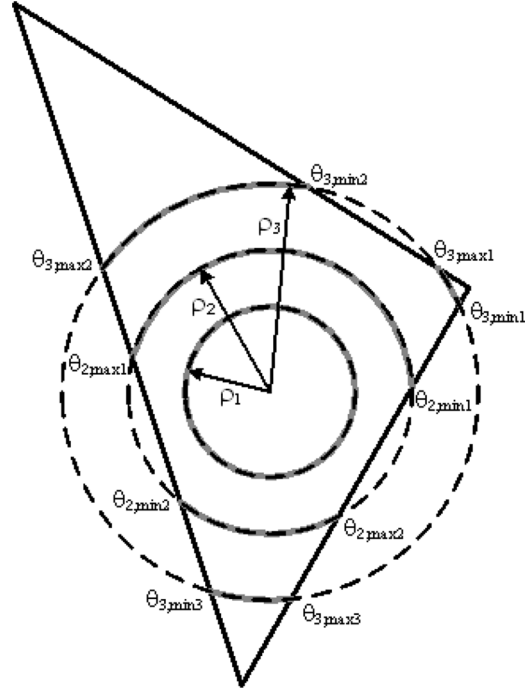


Fig. 3.  $\theta$  integration regions for three different values of  $\rho$  on a triangle.

where  $K(\rho)$  is 1, 2, or 3 depending on  $\rho$ . Substituting (18a), (18b), and (20) into (16b) and (16a) gives

$$\mathbf{M}_{vect} = \int_{\rho_{min}}^{\rho_{max}} \varphi_{M,vect}(\rho) [\hat{\mathbf{u}} \xi_c(\rho) + \hat{\mathbf{v}} \xi_s(\rho)] d\rho \quad (21a)$$

$$M_{scal} = \int_{\rho_{min}}^{\rho_{max}} \varphi_{M,scal}(\rho) \xi_0(\rho) d\rho. \quad (21b)$$

So the original 2-D integration in  $u$  and  $v$  has been reduced to a 1-D integral in  $\rho$ , and the singularity has been removed. The integration in  $\rho$  can easily be computed with a 1-D Gauss-Legendre quadrature rule.

Unlike other integration methods designed to deal with the spatial integration, the polar method is optimized to integrate in space-time. This leads to the calculation of much more efficient and accurate potential calculations.

### III. NUMERICAL RESULTS

In this section, the time-domain polar integration scheme is used to compute the electric scalar and magnetic vector potentials at a point due to a half-RWG function on a single triangle. The method is compared to 2-D Gaussian quadrature using 1, 7, and 25 points with singularity extraction. In all cases, the source triangle has vertices  $(0,0,0)$ ,  $(1,0,0)$ , and  $(0,1,0)$ , where the units are in millimeters.

In the first example, Fig. 4, the potentials are compared for a relatively broad Gaussian pulse, where  $\sigma = 1$  ps. Other than 1-point Gaussian quadrature, all methods accurately predict the shape of the curve and no spurious high-frequency components are present. When elements are electrically small, the polar method is not needed.

Fig. 5 shows the potentials produced by negative Gaussian pulses with mean standard deviation  $\sigma$ . In Fig. 5(a) and (b),  $\sigma = 0.1$  ps. Fig. 5(c) and (d) show the results from a wider pulse where  $\sigma = 0.2$  ps. As can be seen in the figures, when the  $P(t)$  pulse is narrow, the Gaussian schemes do not accurately integrate (21). However, when the  $P(t)$  pulse is wide, higher-order Gaussian schemes work very well, to the extent that the 25-point Gaussian curve is nearly indistinguishable

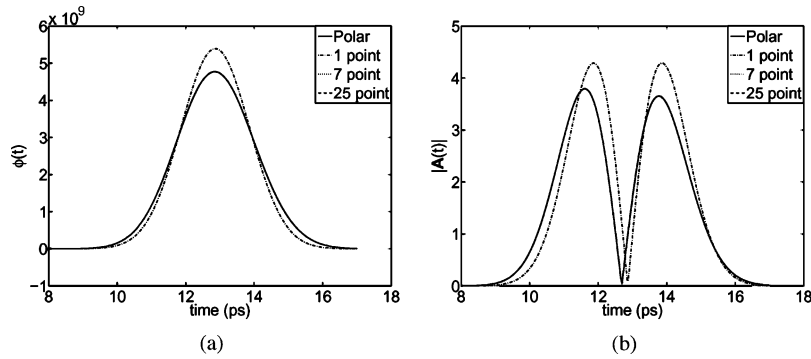


Fig. 4. Potentials from a negative Gaussian pulse with standard deviation  $\sigma = 5$  ps. The source triangle has vertices  $(0,0,0)$ ,  $(1,0,0)$ , and  $(0,1,0)$ , and the observation point is  $(2,2,0)$ , where all positions are measured in millimeters, (a)  $\phi(t)$ , (b)  $|A(t)|$ . Because the triangles are electrically-small, all methods except 1-point Gaussian are sufficient to predict the shape of the potentials.

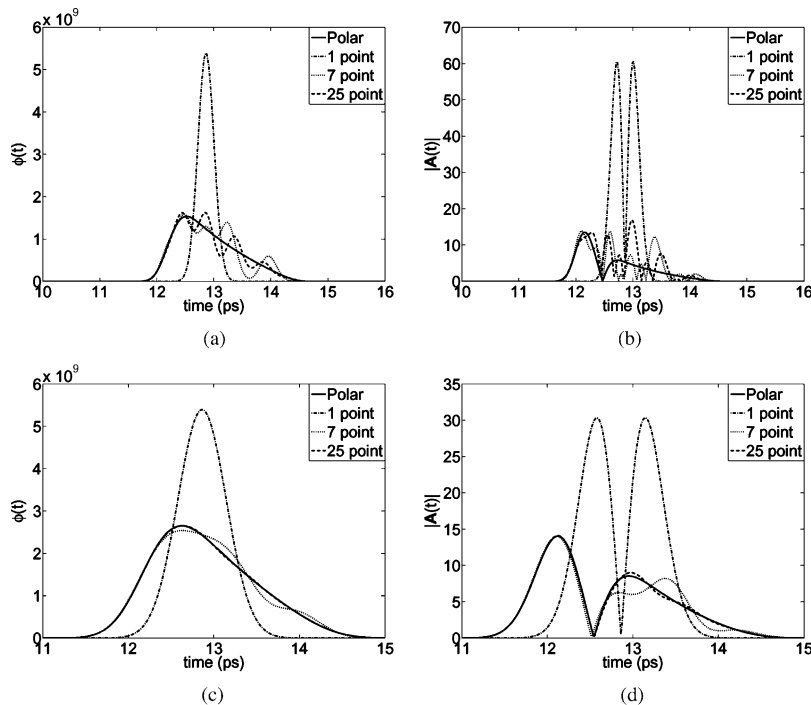


Fig. 5. Potentials from a negative Gaussian pulse with standard deviation  $\sigma$ . The source triangle has vertices  $(0,0,0)$ ,  $(1,0,0)$ , and  $(0,1,0)$ , and the observation point is  $(2,2,0)$ , where all positions are measured in millimeters. (a)  $\phi(t)$  :  $\sigma = 0.1$  ps, (b)  $|A(t)|$  :  $\sigma = 0.1$  ps, (c)  $\phi(t)$  :  $\sigma = 0.2$  ps, (d)  $|A(t)|$  :  $\sigma = 0.2$  ps. In (c) and (d), the 25-point line is nearly indistinguishable from the polar integration result.

from the polar integration curve in Fig. 5(c) and (d). The reason for this is that Gaussian quadrature is designed to integrate slowly-varying, polynomial functions. When the integrand exhibits rapid variations, an extremely high-order Gaussian scheme is required to integrate accurately.

The most critical application of the polar integration scheme is for singular or very-near singular integrations, shown in Fig. 6, where it is compared to Gaussian quadrature with singularity extraction. As can be seen in Fig. 6(c) and (d), the Gaussian quadrature schemes do not show adequate convergence, even when the  $P(t)$  pulse is wide. In all cases the Gaussian scheme gives undue weight to the response at the centroid, giving a maximum where the input signal is a maximum, instead of when nearby responses have propagated to the observer.

Finally, Fig. 7 shows the fall of a negative square pulse, where the rise and fall are modeled with half-sinc functions. Convergence can be seen as higher-order Gaussian schemes are used, approaching the results from polar integration. The small negative error seen in the 1-point line of Fig. 7(c) results from inaccurate quadrature

of the non-singular part of the integral. This error decreases as the Gaussian order increases. Fig. 7(c) and (d) in particular show more accurate integration schemes picking up contributions closer to the triangle edge. The waveform is also much more smooth than the Gaussian quadrature schemes.

It is important to note that in each case above, the area under the group of curves is the same (within 2%). However, the shape of the potential curves is of critical importance. Integrating efficiently in delay places interactions appropriately in the time history, and removes spurious high frequencies from the potentials. Fig. 4 shows that Gaussian integration is suitable for electrically small source elements, producing results identical to polar integration. However, when the interactions become more explicit, polar integration method is required to capture the shape of the potential interactions.

Fig. 8 shows simulations run on a 1-meter cube, modeled with 48 unknowns, using polar quadrature and Duffy's method. Because it is optimized to compute the shape of the potentials, polar integration provides stability at a much smaller time step than Duffy's method.

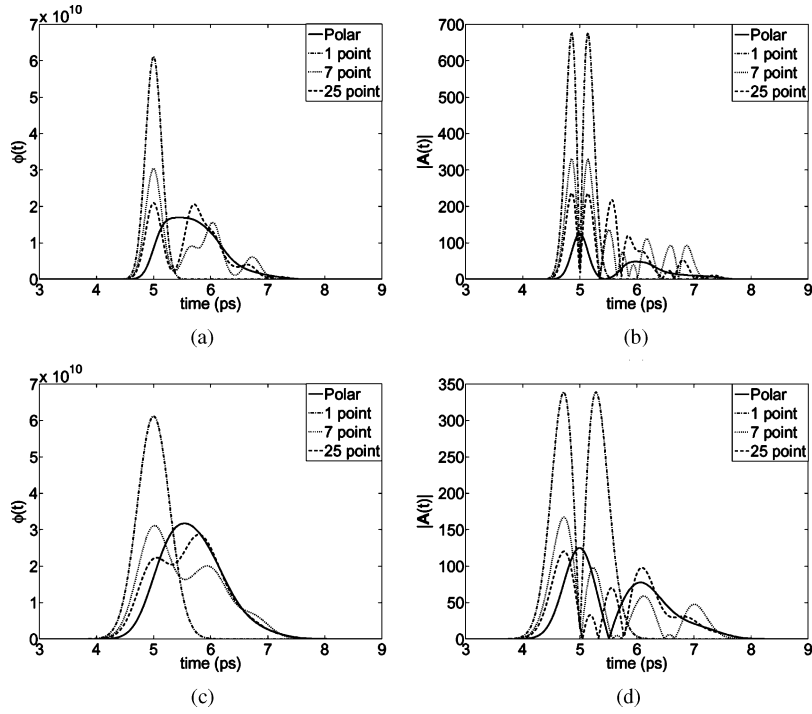


Fig. 6. Potentials from a negative Gaussian pulse with standard deviation  $\sigma$ . The figure compares polar integration to Gaussian quadrature with singularity extraction. The source triangle has vertices  $(0,0,0)$ ,  $(1,0,0)$ , and  $(0,1,0)$ , with the observation point at  $(1/3,1/3,0)$  (the triangle centroid), where all distances are measured in millimeters. (a)  $\phi(t)$  :  $\sigma = 0.1$  ps, (b)  $|A(t)|$  :  $\sigma = 0.1$  ps, (c)  $\phi(t)$  :  $\sigma = 0.2$  ps, (d)  $|A(t)|$  :  $\sigma = 0.2$  ps.

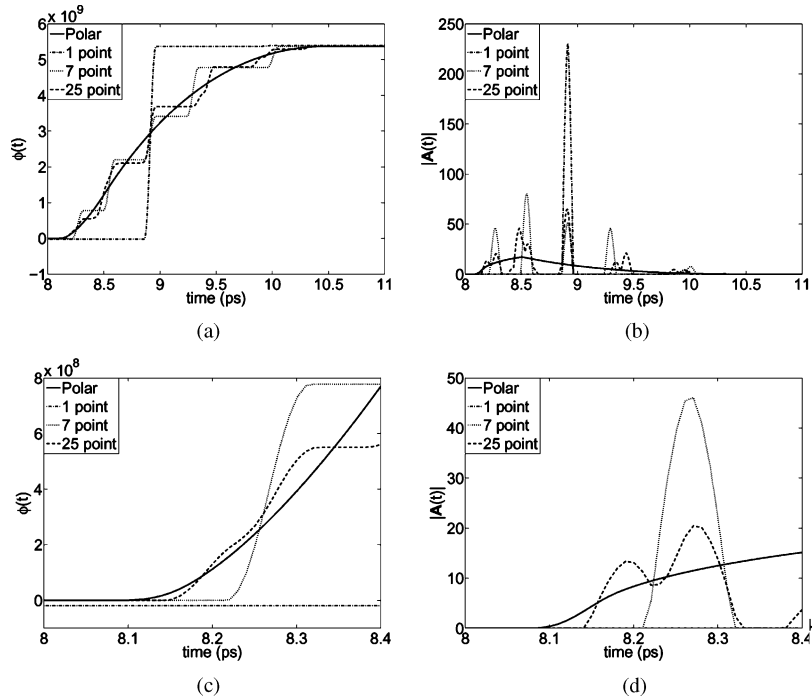


Fig. 7. Potentials from a 9 ps negative square pulse with 0.1 ps rise/fall time, using various quadrature schemes. The source triangle has vertices  $(0,0,0)$ ,  $(1,0,0)$ , and  $(0,1,0)$ , and the observation point is  $(2,2,0)$ , where all distances are measured in millimeters. (a)  $\phi(t)$ , (b)  $|A(t)|$ , (c) zooming in on front of pulse for  $\phi(t)$ , (d) zooming in on front of pulse for  $|A(t)|$ .

IV. CONCLUSION

The polar integration scheme developed in [11] has been adapted to the time-domain and applied to computing magnetic vector and electric scalar potentials. Examples have been presented comparing the scheme

to Gaussian quadrature rules of increasing order using singularity extraction. In summary, polar integration is necessary for cases where the temporal function exhibits rapid variations (with respect to propagation time across the source triangle), and for singular (or nearly-singular) observation points. The polar scheme is especially attractive because

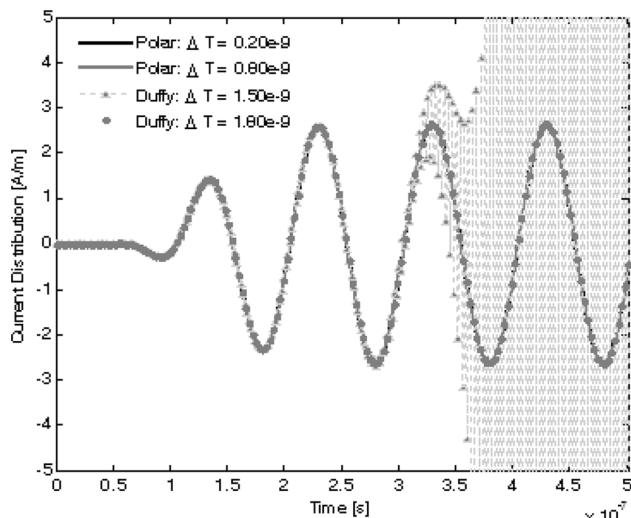


Fig. 8. This figure shows an example run on a unit cube. Polar quadrature enables stability at a much smaller time step than Duffy's method.

the integrand is rendered non-singular, and the integration becomes one dimensional. In addition, polar integration is equally applicable to all interactions, near and far. Finally, because the numerical integration is one dimensional, it is easy to adaptively integrate the potentials to arbitrary accuracy.

As the authors were preparing for final submission upon completion of the review process for this paper, a similar paper [13] entered the literature. While the technique is very similar to the method presented in this paper, it does not address the temporal shape of potential curves as related to stability. Therefore, we believe this paper still represents a significant contribution to the community.

#### ACKNOWLEDGMENT

The authors would like to thank J. Rockway, B. Fasenfest, and D. White of Lawrence Livermore National Laboratory for their assistance in testing the ideas presented in this paper.

#### REFERENCES

- [1] Y.-S. Chung, T. K. Sarkar, B. H. Jung, M. Salazar-Palma, Z. Ji, S. Jang, and K. Kim, "Solution of time domain electric field integral equation using the Laguerre polynomials," *IEEE Trans. Antennas Propag.*, vol. 52, no. 9, pp. 2319–2328, Sep. 2004.
- [2] D. S. Weile, G. Pisharody, N.-W. Chen, B. Shanker, and E. Michielssen, "A novel scheme for the solution of the time-domain integral equations of electromagnetics," *IEEE Trans. Antennas Propag.*, vol. 52, no. 1, pp. 283–295, Jan. 2004.
- [3] G. Manara, A. Monorchio, and R. Reggiannini, "A space-time discretization criterion for a stable time-marching solution of the electric field integral equation," *IEEE Trans. Antennas Propag.*, vol. 45, no. 3, pp. 527–532, Mar. 1997.
- [4] M. J. Bluck and S. P. Walker, "Time-domain BIE analysis of large three-dimensional electromagnetic scattering problems," *IEEE Trans. Antennas Propag.*, vol. 45, no. 5, pp. 894–901, May 1997.
- [5] M. Abramowitz and I. Stegun, Eds., *Handbook of Mathematical Functions*. New York: Dover, 1977.
- [6] D. R. Wilton, S. M. Rao, and A. W. Glisson, *Electromagnetic Scattering by Arbitrary Surfaces*. Rome Air Development Center, Griffiths AFB, NY, Tech. Rep. RADC-TR-79-325, Mar. 1980.
- [7] M. G. Duffy, "Quadrature over a pyramid or cube of integrands with a singularity at a vertex," *SIAM J. Numer. Analysis*, vol. 19, no. 6, pp. 1260–1262, Dec. 1982.
- [8] R. A. Wildman and D. S. Weile, "Two-dimensional transverse-magnetic time-domain scattering using the Nyström method and bandlimited extrapolation," *IEEE Trans. Antennas Propag.*, vol. 53, no. 7, pp. 2259–2266, Jul. 2005.

- [9] M. A. Khayat and D. R. Wilton, "Numerical evaluation of singular and near-singular potential integrals," *IEEE Trans. Antennas Propag.*, vol. 53, no. 10, pp. 3180–3190, Oct. 2005.
- [10] M. J. Bluck, M. D. Pocock, and S. P. Walker, "An accurate method for the calculation of singular integrals arising in time-domain integral equation analysis of electromagnetic scattering," *IEEE Trans. Antennas Propag.*, vol. 45, no. 12, pp. 1793–1797, Dec. 1997.
- [11] S. Chakraborty and V. Jandhyala, "Evaluation of Green's function integrals in conducting media," *IEEE Trans. Antennas Propag.*, vol. 52, no. 12, pp. 3357–3363, Dec. 2004.
- [12] S. M. Rao, D. R. Wilton, and A. W. Glisson, "Electromagnetic scattering by surfaces of arbitrary shape," *IEEE Trans. Antennas Propag.*, vol. 30, no. 3, pp. 409–418, Mar. 1982.
- [13] A. C. Yücel and A. A. Ergin, "Exact evaluation of retarded-time potential integrals for the RWG bases," *IEEE Trans. Antennas Propag.*, vol. 54, no. 5, pp. 1496–1502, May 2006.

## Managing Topological Prioritization in Ray-Tracing Based Progressive Propagation-Prediction Modeling

Antonis G. Dimitriou and George D. Sergiadis

**Abstract**—In a progressive propagation prediction model, significant time is saved by interrupting the process when specific application related constraints have been met. Such limitations have to do with the statistics of intermediate results as well as their spatial arrangement in the area of interest. We propose a time-efficient method to control the topological distribution of intermediate predictions. The proposed criterion allows different priorities to be set in different regions of the study area. In addition, we put forward two progressive strategies capable of adjusting the ray-tracing engine to the desired prioritization. The advantages of the proposed strategies compared with existing approaches are well demonstrated.

**Index Terms**—Progressive propagation modeling, radiocoverage, ray-tracing.

#### I. INTRODUCTION

Traditional empirical or semi-deterministic propagation prediction models have been replaced by deterministic ones based on a combination of geometrical optics and the uniform theory of diffraction, [1]–[3]. The running-time of such models is very important, as mirrored in the efforts after the early 1990s that focus on accelerating the performance of the early models. At the same time, different applications require diverse characteristics concerning the predictions delivered by these models. Significant time could be saved if such a prediction process could be stopped when specific demands, regarding the final results have been safely satisfied.

In a progressive prediction model, intermediate results are continuously fed back to the user, who can stop the prediction process when the specific-application-related required constraints have been met. The concept of progressiveness in ray-tracing propagation prediction models was introduced in [4]. The authors set the basic rules that govern such models. They state that ray-paths should be traced in

Manuscript received September 21, 2005; revised April 5, 2006.

The authors are with the Aristotle University of Thessaloniki, School of Engineering, Department of Electrical and Computer Engineering, Telecommunications Laboratory, Thessaloniki GR-54124, Greece (e-mail: antodimi@mri.ee.auth.gr; sergiadi@auth.gr).

Digital Object Identifier 10.1109/TAP.2006.882197